Fracture 1977, Volume 1, ICF4, Waterloo, Canada, June 19 - 24, 1977

FAILURE MAPS APPLIED TO METAL DEFORMATION PROCESSES

J. D. Embury* and G. H. LeRoy*

ABSTRACT

In describing the failure of metals in forming operations, it is necessary to consider both the operative state of stress and the mechanism of failure in relation to the microstructure. An experimental program has been conducted to measure the strain to failure for various aluminum alloys subject to different loading paths. If it is assumed that the strain history to failure can be described by a sequence of proportional straining and plane strain deformation the fracture condition for any loading path can be expressed either in stress or strain space in the form of a fracture map, the shape of which depends on the fracture mode. This formalism has been used to compare fracture in various materials and microstructural conditions, to illustrate empirical failure criteria and to develop failure criteria for multi-axial loading.

INTRODUCTION

The performance of materials in sheet metals forming operations is usually described by reference to the work hardening characteristics or the plastic anisotropy of the material. Much technological evidence exists to indicate that materials successfully deformed in drawing operations require a high Average strain ratio [1,2,3], (Figure 1). However, for many forming operations which involve deformation in the presence of imposed strain gradients the performance of the material correlates with tensile fracture properties of the material such as the measured reduction in area [4] as illustrated by the example in Figure 2. This is certainly not a universally applicable correlation but is of value for materials of limited ductility, e.g., HSLA steels and high strength aluminium alloys.

Thus, in attempting to compare the behaviour of materials in forming operations we have the inherent difficulty of utilizing the entire strain history of the material which involves both the description of the limit of stable flow which the material can sustain and the fracture of the material. This means that parameters derived from the rather limited strain history available in the uniaxial tensile test are of dubious value in applying to large strain ranges. This lends emphasis to current attempts to derive information from instrumented bulge tests [5] and other large strain deformation processes. Even if we ignore problems such as the influence of lubrication and flow rate the problem is still complex in that both the stability and the fracture process are determined both by stress state and the detailed microstructure.

*Department of Metallurgy and Materials Science, McMaster University, Hamilton, Ontario, Canada.

It is of value to illustrate this premise because it is of major importance in attempting to bridge the disciplines of solid mechanics and physical metallurgy. Consider first the problem of describing the stability of flow or the localisation of strain. If it is assumed that the power hardening law $\sigma_1 = K\varepsilon_1^n$ derived for tensile deformation is valid for all loading paths then following Backhofen [6] we can express the equivalent strain to attain instability, i.e., the maximum load condition, $\bar{\varepsilon}$ as

$$\bar{\varepsilon} = n/g$$

where g is a constant. Typical values of g and the tensile strain to instability for various loading methods are summarised in Table 1.

In addition to the method of loading the onset of unstable flow may be determined by temperature or microstructural features which can result in strain softening [7,8] or the development of negative strain rate sensitivity of the material [9]. An example is shown in Figure 3 for a structural aluminum alloy.

Similarly the strain to failure and the mode of failure is a function of stress state. The practical aspects of the problem are illustrated by Figure 4 which indicates that in forming an aluminum alloy failure may occur either by a predominantly tensile mode or by in-plane shear. The determination of ductility as a function of stress state and its rationalisation in terms of microstructural parameters is a major impediment to the development of an adequate description of the permissible strain distributions at crack tips and is exemplified by the data shown in Figure 5.

Thus, the ability to rationalise and portray the limits of stable flow and the process of failure as a function of stress state would represent a useful method for comparing the behaviour of materials at large imposed strains. In the present work an attempt is made to portray the behaviour of sheet materials at large plastic strains. It is in principle possible to extend the treatment but currently little experimental data is available for materials tested at large imposed pressures and the essential physical processes of void nucleation and growth and local failure are not sufficiently clearly elucidated to provide a genetal framework for comparison of materials. A very useful method of representing the behaviour of sheet materials is the forming limit diagram introduced by Keeler and Backhofen [10], Figure 6. This diagram is an empirical diagram which represents the maximum level of useful strain, the limit strain, which can be imposed in any combined stress state prior to localised necking in the sheet.

Figure 6 illustrates the idealised modes of deformation which a material could undergo if deformed along a particular path in which the strains were linearly proportional. After the onset of strain localisation we can imagine in the idealised case the material forms a groove which continues to deform by an approximately plane strain path up to failure. Thus, a second envelope can be added to the diagram representing the strain to failure of the material for a particular strain path, i.e., we approximate the process by a combined path in which we have proportional straining up to instability followed by a period of plane strain deformation (Figure 6). Experimental data to describe the position of the limit strain and failure can be determined from the measurement of grids on the surface of a deforming sheet plus measurements of the thickness strains at failure. Careful analysis of the distribution of strains in fractured samples enable the importance of strain gradients to be determined and the approximation of the consecutive strain paths described above to be validated. Typical

examples of the strain measuring grids are shown in Figure 7 (Hecker cup tests). These tests need to be complimented by tensile ($\sigma_2 = 0$), bulge ($\sigma_1 = \sigma_2$) and in-plane torsion tests, in order to determine the basic mechanical properties of the material.

In any fracture process there is the inherent problem of specifying the critical event determining the onset of failure. In many cases justification can be given for either a stress based criterion or a strain based criterion and thus it is of value to consider the representation of the stability and failure conditions in both strain and stress co-ordinate systems. In essense this results in the production of a *failure map which is capable of representing the entire strain history of the sample for a variety of stress states.* However, in order to transpose the experimental data concerning the observed strain values into other co-ordinate systems we must impose a series of premises concerning both the straining conditions and the continuum description of the material.

STRESS AND STRAIN RELATION

The calculations which follow relate stress and strain for sheet materials obeying a simple formulation of macroscopic anisotropy and deformed in proportional loading, plane stress processes.

1) Choice of an equivalent stress function

Hill's analysis for anisotropy leads to a function of the form

$$\begin{cases} \bar{\sigma}^2 = \sigma_1^2 + a\,\sigma_1\sigma_2 + b\sigma_2^2 \\ \sigma_3 = 0 \end{cases} \qquad (1)$$

where a and b are constants which can be obtained from the strain ratios measured in uniaxial tests in the rolling and transverse direction of the sheet respectively. In this theory, it is assumed that a hydrostatic stress does not influence yielding.

2) Associated flow rule

The normality rule: $d\varepsilon_{ij} = d\lambda \left(\frac{\partial\bar{\sigma}}{\partial\sigma_{ij}}\right)$ can here be written using the condition of volume constancy

$$d\varepsilon_1 + d\varepsilon_2 + d\varepsilon_3 = 0 \qquad (2)$$

$$\frac{d\varepsilon_1}{2\sigma_1 + a\,\sigma_2} = \frac{d\varepsilon_2}{2b\,\sigma_2 + a\,\sigma_1} = \frac{d\varepsilon_3}{-(2+a)\,\sigma_1 - (2b+a)\,\sigma_2} = \frac{d\bar{\varepsilon}}{2\bar{\sigma}} \qquad (3)$$

3) Derivation of the equivalent strain function

The expression of $d\bar{\varepsilon}$ can be obtained from (3) and the definition of $\bar{\sigma}$ (1). The identification leads to the result:

$$(d\bar{\varepsilon})^2 = \frac{4}{4b-a^2}\left(b\,d\varepsilon_1^2 - a\,d\varepsilon_1\,d\varepsilon_2 + d\varepsilon_2^2\right) \qquad (4)$$

4) Straining condition

Assuming proportional straining:

$$\frac{d\varepsilon_1}{d\varepsilon_2} = \frac{\varepsilon_1}{\varepsilon_2} = \ell \tag{5}$$

Relation (3) gives proportional loading condition with a slope m defined by:

$$m = \frac{\sigma_1}{\sigma_2} = \frac{a - 2b\ell}{a\ell - 2} \tag{6}$$

The introduction of ℓ and m into (1) and (4) leads to the simplified expressions:

$$\bar{\sigma} = \left(1 + \frac{a}{m} + \frac{b}{m^2}\right)^{1/2} \sigma_1 \tag{7}$$

$$\bar{\varepsilon} = \frac{4}{4b-a^2}\left(b - \frac{a}{\ell} + \frac{1}{\ell^2}\right)^{1/2} \varepsilon_1 \tag{8}$$

5) Choice of a material law

From the model we can propose a relation of the form

$$\bar{\sigma} = K\,\bar{\varepsilon}^n \tag{9}$$

6) Mapping strain and stress states

Starting from strain measurements which can be made directly on a deformed part, we can calculate the corresponding points in the stress space. The sequence of operations is given below:

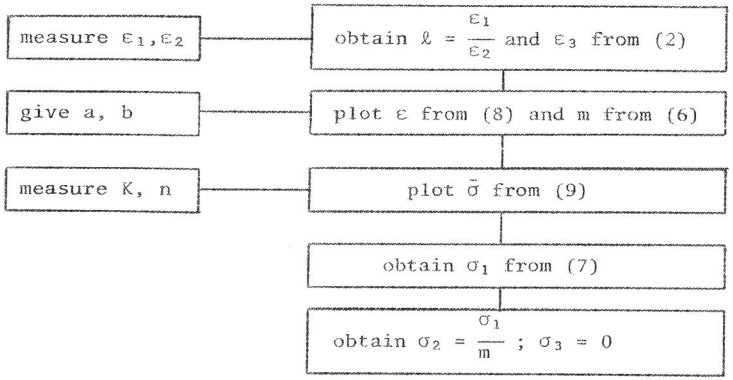

Schematically:

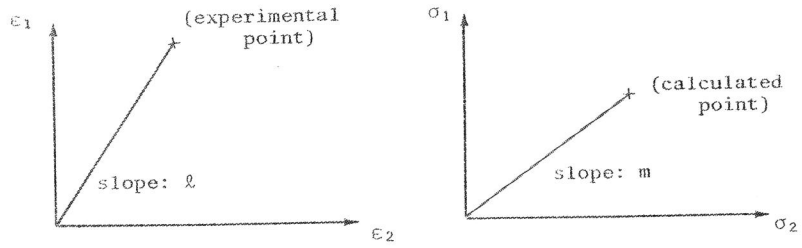

Let us now consider the application to the various cases commonly found in practice:

A. *Isotropic materials:*

In that case, the Von Mises or distortional energy criterion can be written:

$$\bar{\sigma} = \sigma_1^2 - \sigma_1\sigma_2 + \sigma_2^2$$

Replacing a and b by -1 and 1 respectively, one finds the familiar expressions,

$$\bar{\sigma} = \left(1 + \frac{1}{m^2} - \frac{1}{m}\right)\sigma_1$$

$$\bar{\varepsilon} = \frac{2}{\sqrt{3}}\left(1 + \frac{1}{\ell^2} + \frac{1}{\ell}\right)^{1/2} \varepsilon_1$$

$$m = \frac{2p + 1}{p + 2}$$

B. *The planar isotropy case:*

Assuming that the normal anisotropy coefficient R remains constant during straining, we can use the expression proposed by Hill [11]

$$\bar{\sigma}^2 = \sigma_1^2 - \frac{2R}{1+R}\sigma_1\sigma_2 + \sigma_2^2$$

Replacing a and b by $-\frac{2R}{1+R}$ and 1 respectively:

$$\bar{\sigma} = \left(1 - \frac{2R}{1+R}\frac{1}{m} + \frac{1}{m^2}\right)^{1/2} \sigma_1$$

$$\bar{\varepsilon} = \frac{1+R}{\sqrt{1+2R}}\left(1 + \frac{2R}{1+R}\frac{1}{\ell} + \frac{1}{\ell^2}\right)^{1/2} \varepsilon_1$$

$$m = \frac{(1+R)\ell + R}{R\ell + (1+R)}$$

C. *The anisotropic case:*

For anisotropic materials, the constants a and b have been related to the strain ratios:

$$r = \frac{\varepsilon_w}{\varepsilon_t}$$

measured in the rolling direction (r_o) and the transverse direction (r_{90}) [12]

$$\bar{\sigma}^2 = \sigma_1^2 - \frac{2}{C}\sigma_1\sigma_2 + \frac{B}{C}\sigma_2^2$$

where $$B = \frac{1 + r_{90}}{r_{90}}, \quad C = \frac{1 + r_o}{r_o}$$

The relations can be written in that case:

$$\bar{\sigma} = \left(1 - \frac{2}{C} \cdot \frac{1}{m} + \frac{B}{C} \cdot \frac{1}{m^2}\right)^{1/2} \sigma_1$$

$$\bar{\varepsilon} = \left(\frac{C}{BC-1}\right)^{1/2}\left(B + \frac{2}{\ell} + \frac{C}{\ell^2}\right)^{1/2} \varepsilon_1$$

$$m = \frac{B\ell + 1}{\ell + C}$$

Example

The forming limit diagram determined from fracture strain measurements has been determined (Figure 8) in the case of an Al-Mg alloy (5154), in which the mechanical properties are approximately the same in the rolling and transverse directions (yield strength=19 Ksi, U.T.S. = 38 Ksi; n = 0.32). In the Hecker cup test, the strain gradient in the ε_1 direction perpendicular to the void was found to be very important for strains in the range $-2 \leq \ell \leq 0$, (formation of a local neck), while the gradient reduces to zero as $\bar{\ell} \to \bar{1}$ (no necking before fracture). The strain gradient in the ε_2 direction (parallel to the crack) was always very small near the fracture site (plane strain conditions). The choice of straining paths indicated in Figure 8 was based on these observations.

After collecting all the necessary data, the equations developed earlier were used to calculate the limit and fracture maps, i.e., equivalent of the limit strain and fracture strain curves in the stress space (Figure 9).

The level and the shape of the two maps depict two main features:

1) The stress at failure related to the yield stress, for a wide range of loading paths.
2) The locus of failure (fracture map) related to the locus of instability (limit map).

The knowledge of both the position of these two curves in the stress space and their relative separation can serve as a basis for the comparison of materials from the point of view of the effect both of the loading paths and the structure.

APPLICATIONS

Having established the basic formalism needed to portray the failure map in stress or strain coordinates we can utilise the formalism for three basic purposes viz a) the comparison of materials, b) establishing the relevance of empirical failure criteria and c) the development of theories of failure for multi-axial loading.

a) Comparison of materials

The ability to describe the entire strain history to failure can be used as a basis for the comparison of material behaviour. This enables a comparison to be made not only in terms of a normalised parameter such as the stress component relative to the initial yield stress but also it enables more general aspects of behaviour to be compared e.g. the relative behaviour of a given material when subject to pure shear or biaxial tension.

In this regard it is germane to comment on the complex shapes of the failure surfaces relative to the initial yield surface. If we consider the strain hardening of the material in terms of the expansion of the yield surface then following Drucker [13] it can be shown that the expanded yield surface remains convex and does not violate the normality rule. A given expanded yield surface is defined at a constant value of plastic work done per unit volume by the deviatoric stress components. However, the total work per unit volume along any loading path to failure is not constant but depends on loading trajectory. An obvious example is in the Griffith theory of failure where the stress for compressive failure is 8 times that to tensile failure [14]. Thus, in general the failure surface is not an expanded yield surface but it connects points on various expanded yield surfaces, i.e. expanded by strain vectors of varying magnitude. Thus, the failure surface may exhibit re-entrant shapes and singularities and is not constrained to mirror the geometry of the initial yield surface.

Obviously tests on sheet materials permit access only to a limited portion of the total failure surface but this is in general sufficient to permit some useful comparisons to be made both between materials and in regard to the influence of heat treatment on a given alloy.

Limit strain data have been collected for 5 different aluminum alloys and one aluminum killed drawing quality steel and are shown directly replotted in the stress space in Figure 10. The shape of the limit maps is not as precise as in the former case, since they are obtained from a few experimental points only, but we are here interested in the stress levels only. The diagrams include measurement in torsion tests recommended by Marciniak [15]: along this axis ($\sigma_1 = -\sigma_2$) the limit and fracture strains coincide.

We notice that the sequence of stress levels along the tensile axes and the balanced biaxial tension axis is the same and is given by that of the yield strengths indicated in the figure, but the sequence is altered in pure shear due to the reduction of ductility of the 2036-T4 alloy in this stress state. The overlap shows that although this material can withstand greater stresses before any visible neck develops in the region where both σ_1 and σ_2 are positive, instability occurs at lower stresses along the pure shear axis.

Additional work would be needed to relate the relative fracture behaviour of these materials to their structure, but the knowledge of the

maps may be used as a preliminary indicator by press-shops in the selection of materials suitable for forming operations which inlcude pure shear deformation modes.

b) Use of failure maps to illustrate empirical fracture criteria

Recent work by the metal forming group at McMaster has considered the use of a variety of coordinate systems to express failure criteria for sheet metals. This work [16] is summarised in the section below. Its objective is to explore in a general way the different phenomena which might influence failure in sheet forming processes and to illustrate graphically the significance of different hypotheses of failure.

There is a variety of possible failure criteria that may be applied to sheet materials although it is to be expected that each criterion will be relevant only to a limited number of materials, metallurgical conditions, forming operations or loading paths. For example, a maximum principal stress criterion may have more relevance to brittle materials or to materials having intergranular weaknesses than a maximum shear stress criterion, which may itself be better applied to ductile materials. Where voiding is a prominent feature of failure it is to be expected that a growth and coalescence criterion involving the hydrostatic stress component might be most appropriate. The essential point here is that no one theory can be expected to hold for wide ranges of materials and testing conditions. Several possible theories may be applicable and determining the relevant one for a given set of circumstances may be difficult.

Let us consider briefly three simple empirical failure criteria and their resultant failure maps.

Maximum principal stress:

If a maximum principle stress criterion [17] is chosen, i.e.

$$\sigma_1 = \text{constant}$$

the failure curve has the form shown in Figure 11(a) with a high failure strain in pure shear, $\sigma_1 = -\sigma_2$, and a minimum failure strain under approximately plane strain deformation. The form of this diagram depends on the value chosen for n, particularly at negative ε_2 values. Under tensile straining conditions, $\sigma_2 = 0$, ε_1 at failure increases with n; however, for conditions of pure shear, the reverse is the case since it may be shown that

$$\frac{\varepsilon_1}{\bar{\varepsilon}_f} = \frac{3}{2}\left(\frac{1}{n} + 1\right)/2$$

where $\bar{\varepsilon}_f$ is the strain to failure in uniaxial tension and the greater is n the smaller is the failure strain.

The stress diagram for this criterion is an obvious one and is shown in Figure 11(b).

In determining the failure map diagrams, the plasticity theory and assumptions indicated previously have been followed but it is assumed that the material obeys the simple stress strain relation given by the law,

$$\bar{\sigma} = K\bar{\varepsilon}^{0.2}$$

In some cases the shape of the curves is dependent on the strain hardening exponent and the value, n = 0.2, was chosen arbitrarily although this is a reasonable value for many common sheet materials. The scale of the diagrams is of crucial importance and this should be the major area of concentration in future studies but in this first attempt we express the diagrams in non-dimensional form. The curves indicate the stress and strain parameters $\sigma_{1,2}/\sigma$ and $\varepsilon_{1,2}/\varepsilon$ at which failure is expected from each theory. σ_1 and σ_2 are the actual principal stresses and ε_1 and ε_2 are the principal strains at failure in a proportional plane stress process and σ and ε are the stress and strain at failure in uniaxial tension.

Maximum thickness strain:

An empirical criterion which is obeyed quite well in forming sheet in processes ranging from simple tension to biaxial tension [12] is that the thickness strain at fracture is constant, i.e.

$$\varepsilon_3 = \text{constant}$$

This is shown in the strain map in Figure 12(a) and the stress diagram, Figure 12(b), which is not unlike the maximum principal stress curve, Figure 11(b), at least for loading paths away from pure shear.

Maximum shear stress:

A maximum shear stress criterion,

$$\tau_{max} = \text{constant}$$

is of interest because failure phenomena appear to be related to strain disturbances along planes of maximum shear. The strain and stress diagrams are shown in Figure 12(a) and (b). In the region in each map between simple tension and biaxial tension, $-1/2 < \varepsilon_2/\varepsilon_1 < 1$ and $0 < \sigma_2 < 1$, the plane of maximum shear is at 45^0 to the surface of the sheet. In the shear region, $\varepsilon_2/\varepsilon_1 < -1/2$, and $\sigma_2/\sigma_1 < 0$, the plane of maximum shear is perpendicular to the surface. From a stability point of view it could be argued that these are two different phenomena as in one case concentrated shear would lead to a loss in the load bearing cross-section and this would not necessarily be true in the other case.

c) The development of fracture criteria for multi-axial loading

One of the essential features in understanding the mechanical behaviour of materials has been elucidation of the microstructural and atomistic factors which influence the competition between fracture and continued plastic flow in solids [18,19]. In many materials this can be expressed as a competition based on the attainment of a critical stress dependent on the temperature of loading and some local microstructural feature of the material such as the grain size, the condition of the grain boundaries or the size of some internal brittle component such as a carbide. An example is given in Figure 13 which illustrates in a simple manner the competition between fracture and flow in iron resulting from modification of the local grain boundary microstructure. A more complex map of the available low temperature failure modes in a heat treatable Al-Zn-Mg is given in Figure 14. Ashby [20] has recently expanded the utilisation of

such maps in stress temperature space to demonstrate the relationships between failure modes at various strain rates. The salient feature of the comparisons shown above is to note that *in general we must take cognisance not only of the competition between plasticity and fracture but also the competition between available fracture modes.* This raises a third mode of utilisation of failure maps viz. the examination of the influence of stress state on the occurrence of a well defined and quantitatively characterised mode of failure. To date little data is available on this aspect although some valuable progress has been made in the discussion of the influence of hydrostatic pressure on the strain to failure resulting from void nucleation and growth [21,22]. However, in sheet materials the detailed physics of failure are not generally established in terms of microstructural variables. Thus, it is useful to illustrate the potential use of the failure maps by heat treating material to promote a given failure mode and then examining the influence of the available strain paths on the resultant failure. Samples of an aluminum alloy 7004 were heat treated as indicated in Table 2 to produce a) peak hardness and b) catastrophic shear failure prior to necking. Samples were then tested in a variety of straining paths and the failure maps established as in Figure 15, which illustrates the difference between conventional ductile failure and the catastrophic shear mode.

A second example is ultra fine grained materials, whose forming behaviour can be compared with conventional materials using failure maps. A fracture map is shown in Figure 16 for an ultra fine grained aluminum alloy of grain size 1 - 2 μm. This should be compared with Figure 9, obtained for a conventional 5154 alloy of similar yield stress.

CONCLUSIONS

This presentation illustrates the basic formalism for the protrayal of the failure behaviour of sheet materials during forming processes. It should be emphasized that the work is at an early stage and is yet not to be regarded as a complete and useful methodology. However, the work indicates that the failure maps may be used both to compare the behaviour of materials e.g. the competition between alloys to form a given component and on a more basic level to extend and compare the failure criteria applicable to sheet metals. The concepts of failure maps can be extended to a more general loading states and in the future the form of the maps may be capable of modification in order to express the work to failure as a function of variables such as pressure or temperature and thus provide a more general formalism for the comparison of the fracture resistance of materials.

ACKNOWLEDGEMENTS

The authors wish to express their sincere thanks to Dr. J. Duncan, Dr. R. Sowerby and other colleagues at McMaster and to Dr. L. M. Brown of the Cavendish Laboratory, Cambridge, for valuable and stimulating discussions. The work reported was generously supported by N.R.C. (Canada) and Alcan International and one of the authors (G. LeRoy) received a research scholarship from Canada Council during the course of this study.

REFERENCES

1. BLICKWEDE, D. J., New Knowledge about Sheet Steel, ASM, Metals Park, Ohio, 1970.
2. LANKFORD, W. T., BAUSCHER, J. A. and SNYDER, S. C., Trans. ASM, 42, 1950, 1197.
3. KEELER, S. P., Sheet Metal Industries, September, 1965.
4. HERO, H., UKO, D. K., FILIPOVIC, A., SOWERBY, R. and DUNCAN, J. L., Metalworking Research Group, McMaster University, Canada, September 1976.
5. DUNCAN, J.L., KOLODZIEJSKI, J. and GLOVER, G., Bulge Testing as an Aid to Formability Assessment, Metalworking Research Group, McMaster University, Canada, January 1976.
6. BACKHOFEN, W. A., Deformation Processing, Addision Wesley, 1972, 214.
7. ARGON, A. S., The Inhomogeneity of Plastic Deformation, ASM, 1973, 161.
8. TANAKA, T. and SPRETNAK, C., Met. Trans., 4, 1973, 443.
9. CHUNG, N., EMBURY, J. D., EVENSEN, J. D., HOAGLAND, R. G. and SARGENT, C. M., Acta. Met. (in press).
10. KEELER, S. P. and BACKHOFEN, W. A., Trans. ASM, 56, 1963, 25.
11. HILL, R., Mathematical Theory of Plasticity, Oxford University Press, 1950.
12. MARCINIACK, Z., Aspects of Material Formability, Metalworking Research Group, McMaster University, Canada, February 1974, 67.
13. DRUCKER, D. C., 1st U.S. Congress of Appl. Mech., ASME, 1952, 487.
14. JAEGER, J. C., Elasticity, Fracture and Flow, Methuen, 1956, 85.
15. MARCINIACK, Z. and KOLODZIEJSKI, J., Proc. of the 7th Biennial Congress of IDDRG, Amsterdam, 1972.
16. GLOVER, G., DUNCAN, J.L. and EMBURY, J. D., Metals Technology (to be published).
17. DORN, J. E., Fracturing of Metals, ASM, 1948, 32.
18. ZENER, C., Fracturing of Metals, ASM, 1948, 3.
19. OROWAN, E., Repts. Prog. Phys., 12, 1948, 185.
20. ASHBY, M. F., Fracture 1977, Ed. D.M.R. Taplin, University of Waterloo Press, 1977.
21. RICE, J. R. and TRACEY, D. M., J. Mech. Phys. Solids, 17, 1969, 201.
22. BROWN, L. M., The Mechanics and Physics of Fracture, Metals Society, London, 1976.
23. CLOKE, W., M. Eng. Thesis, McMaster University, 1975.
24. KAUFMAN, J. G., AGARD Conference proceedings No. 185, Brussels, 1975, p. DA.9.

Table 1 Equivalent strain at instability for various loading paths

Case	q	ϵ_1/n
Internally pressurized sphere ($\sigma_2/\sigma_1 = 1$)	3/2	1/3
Capped cylindrical tube, internally pressurized ($\sigma_2/\sigma_1 = 1/2$; $\sigma_1 = pr/t$)	$\sqrt{3}$	1/2
Open-ended cylindrical tube, internally pressurized ($\sigma_2 = \sigma_3 = 0$; $\sigma_1 = pr/t$)	3/2	2/3
Sheet loaded in its plane, orthogonally and equally ($\sigma_2/\sigma_1 = 1$)	1/2	1
Sheet loaded in its plane, extending in plane strain ($\sigma_2/\sigma_1 = 1/2$)	$\sqrt{3/2}$	1
Rod in tension	1	1

Table 2 Heat treatments performed on the 7004 aluminum alloy

Alloy and temper	Heat treatment
7004 - T6	Solution treated at 748 K for 1 hr + quenched in brine and aged at 393 K for 24 hrs.
7004 - T4	Solution treated at 748 K for 1 hr + quenched in brine

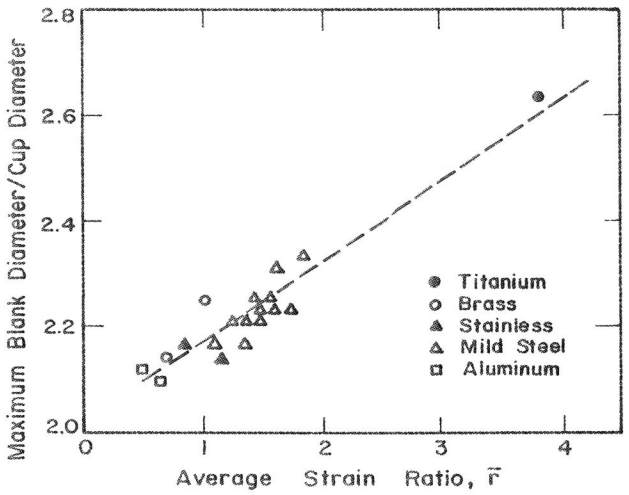

Figure 1 Diagram showing that the average strain ratio $\bar{r}$ is directly related to drawability: the higher the $\bar{r}$ value, the deeper the cup can be formed by pure drawing. Reference [1].

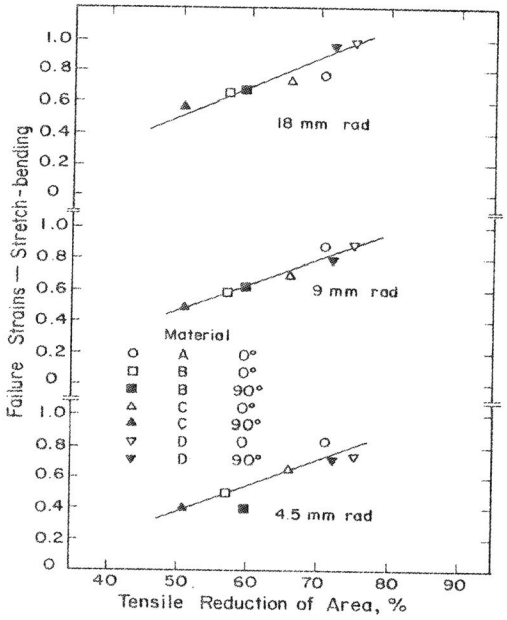

Figure 2 Diagram showing that in the case of forming operations which involve deformation in the presence of imposed strain gradients the performance of the material can correlate with the reduction in area in a tensile test. Data from reference [4].

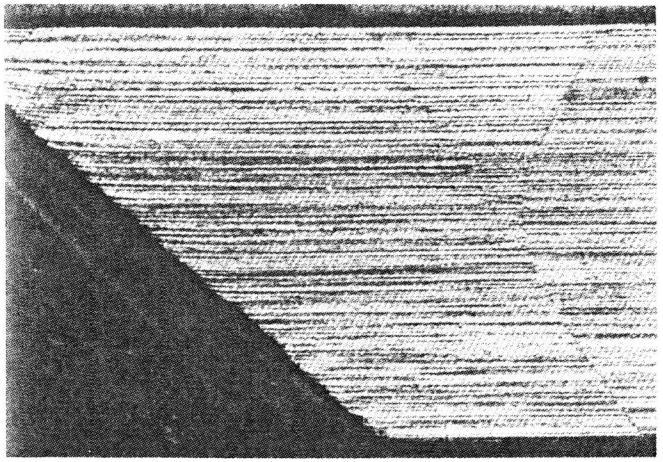

Figure 3 Picture showing the development of intense bands of shear which pass through the entire cross-section of the polycrystal, in the case of an as-quenched 7075 Al alloy tested at room temperature and exhibiting negative strain rate sensitivity. Reference [9].

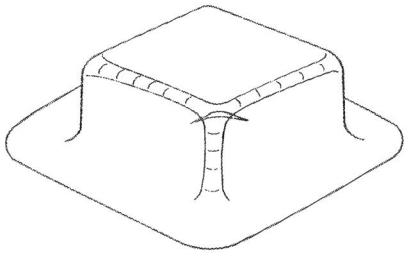

(a) fail at bottom corner, at angle to bottom

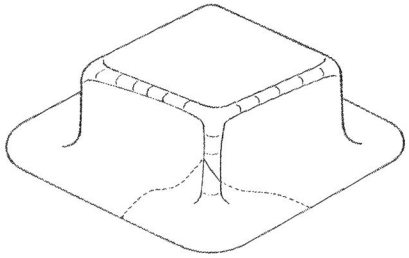

(b) inclined split in side wall at corner, propagate into flange

Figure 4 Sketches illustrating various types of failure observed in square cup tests drawn from circular blanks, in the case of aluminum alloys.

(a) Fail at bottom corner, at angle to bottom.

(b) Inclined split at side wall.
Data from reference [23].

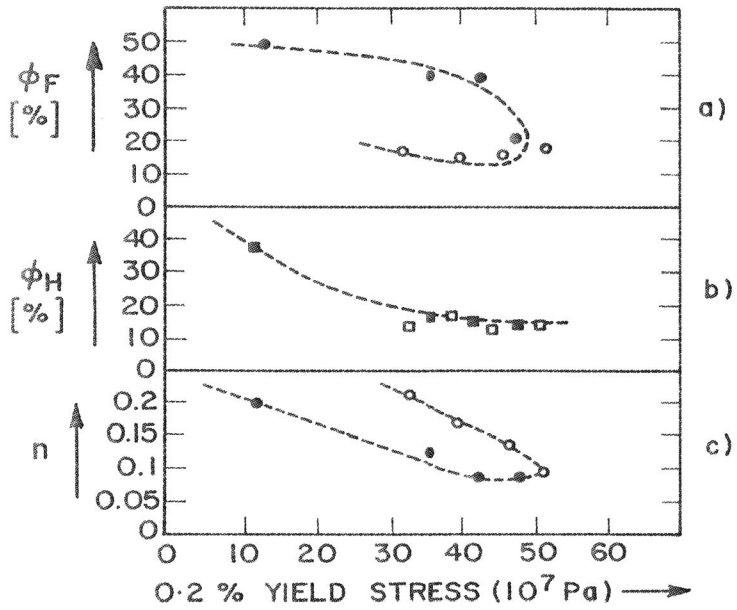

Figure 5 Variation of Uniaxial and plane strain tensile ductility, ϕ_F and ϕ_H respectively, and of strain hardening exponent n for 7075 alloy plate in different aging conditions. Data from reference [24].

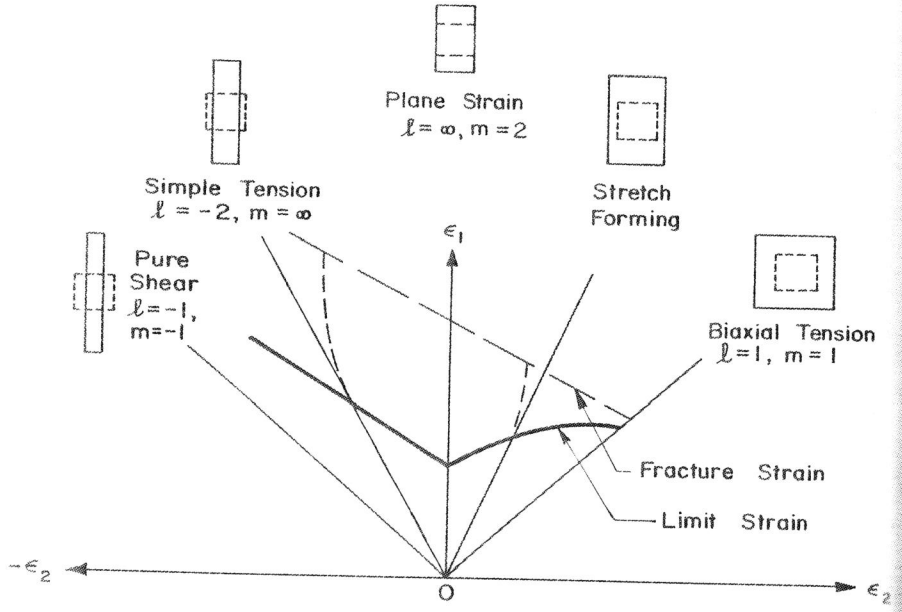

Figure 6 Schematic diagram showing the position of the forming limit strain curve and the fracture strain curve in principal strain space.

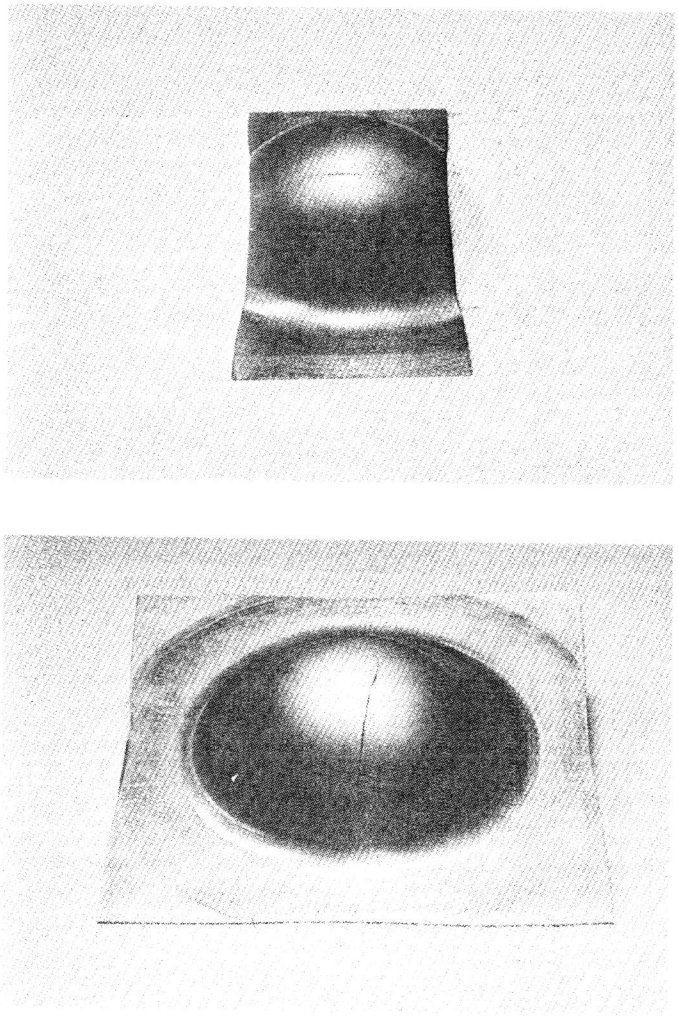

Figure 7 Hecker cup specimens after fracture. Small circles have been initially printed on the blanks. The degree to which the circles are distorted after deformation of the blank provides a measurement of the surface strains ε_1 and ε_2.

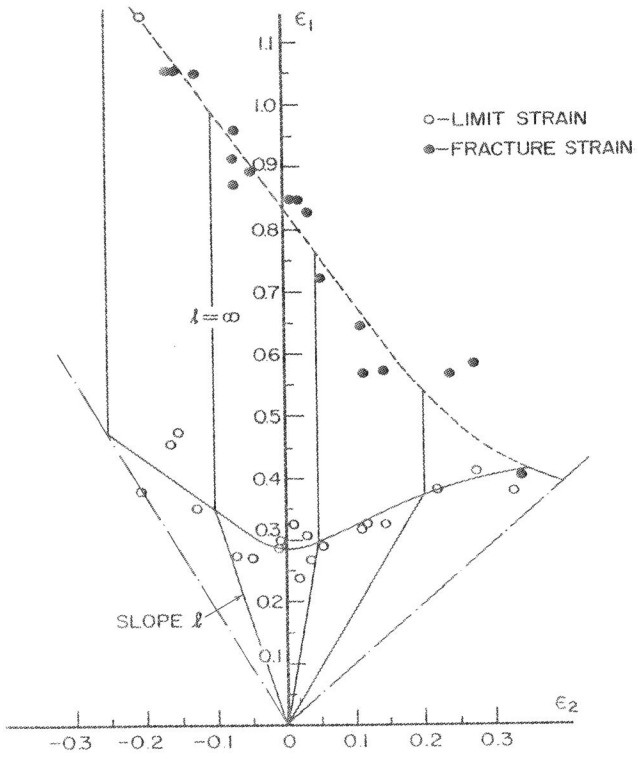

Figure 8 Limit strain curve and fracture strain curve in the case of an Al-Mg alloy (5154) tested at room temperature in the annealed condition. ϵ_1 and ϵ_2 are respectively the major strain and the minor strain in the plane of the sheet.

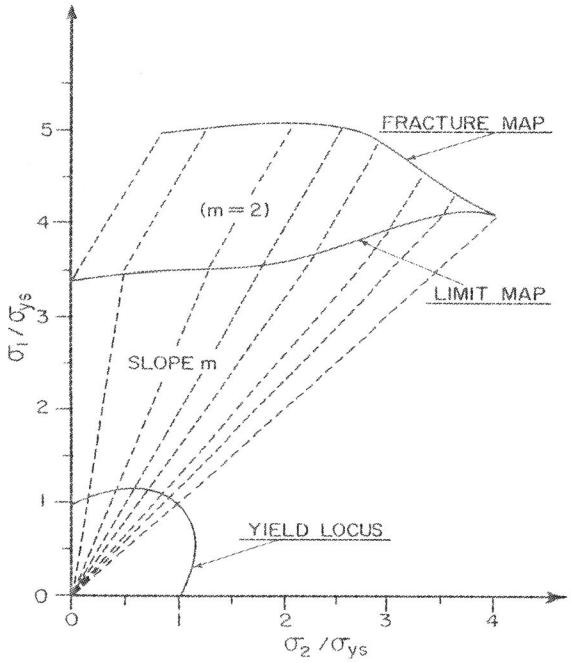

Figure 9 Limit map and fracture map corresponding to the limit strain curve and fracture curve respectively, in axes normalised to the yield stress.

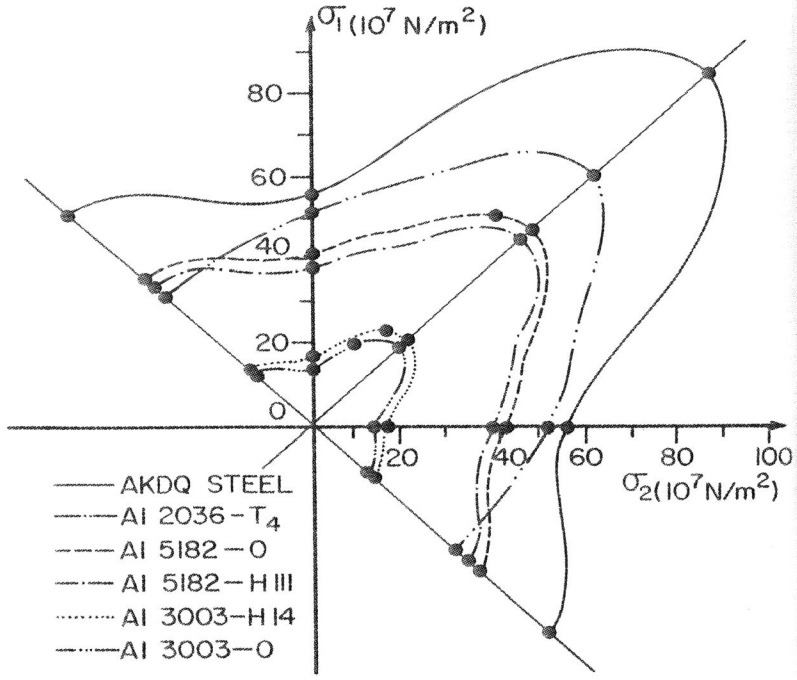

Figure 10 Limit maps for five different aluminum alloys and one aluminum killed drawing quality steel.

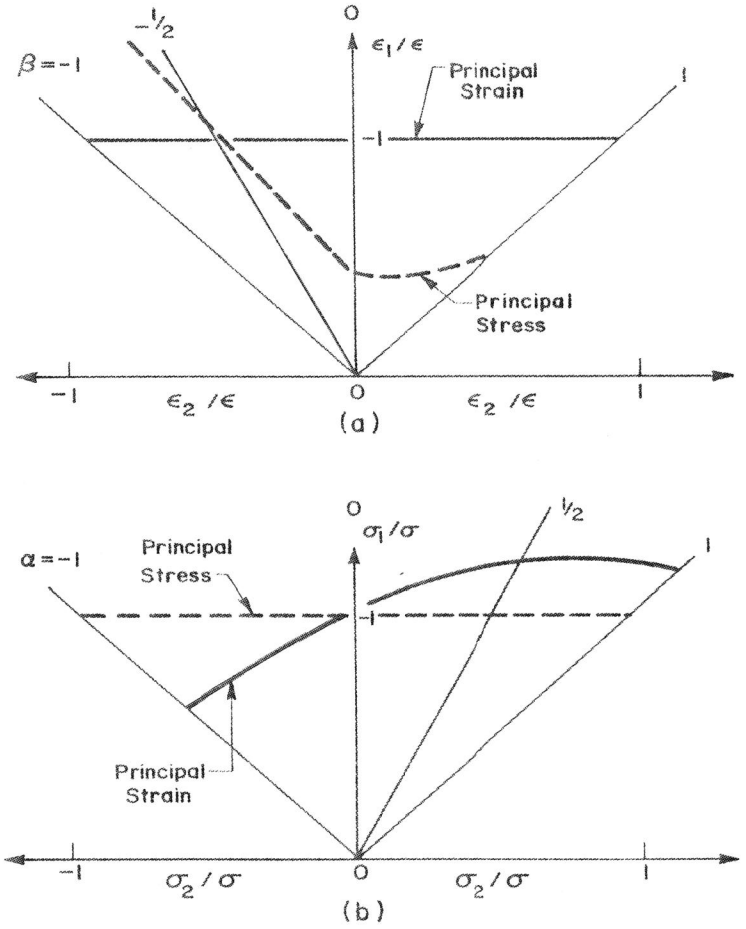

Figure 11 Schematic diagram showing the failure curves for the criterion that the maximum principal strain at failure, ϵ_1, has a constant value (full line) and that the maximum principal stress at failure has a constant value (dashed line).

(a) strain space (b) stress space

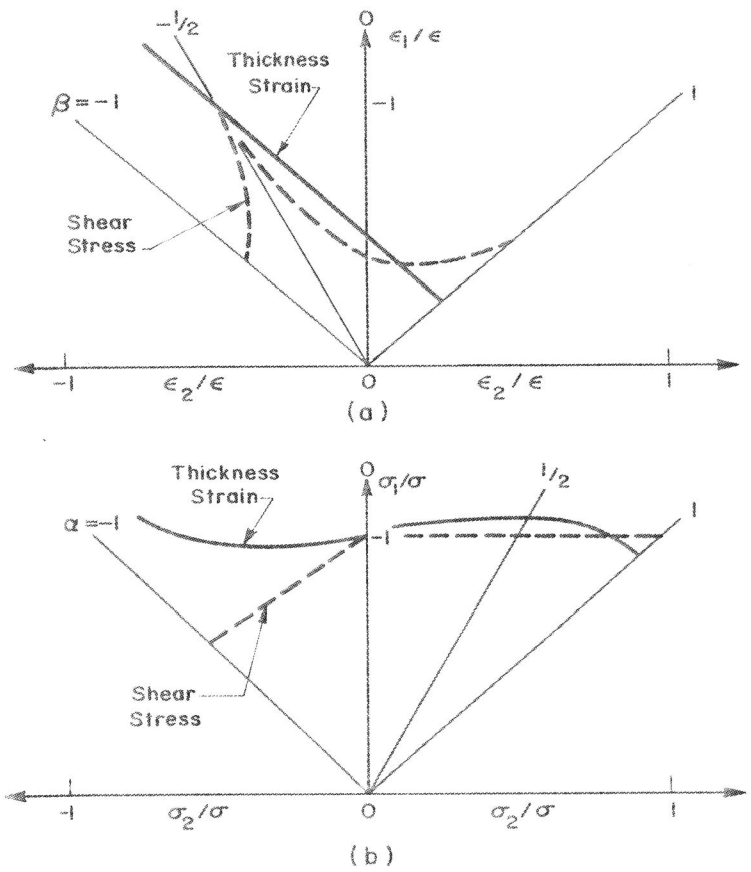

Figure 12 Schematic diagram showing the failure curves for the criteria that the thickness strain at failure, ε_{3f}, has a constant value (full line) and that the maximum shear stress, τ_{max}, has a constant value at failure (dashed line).

(a) strain space (b) stress space

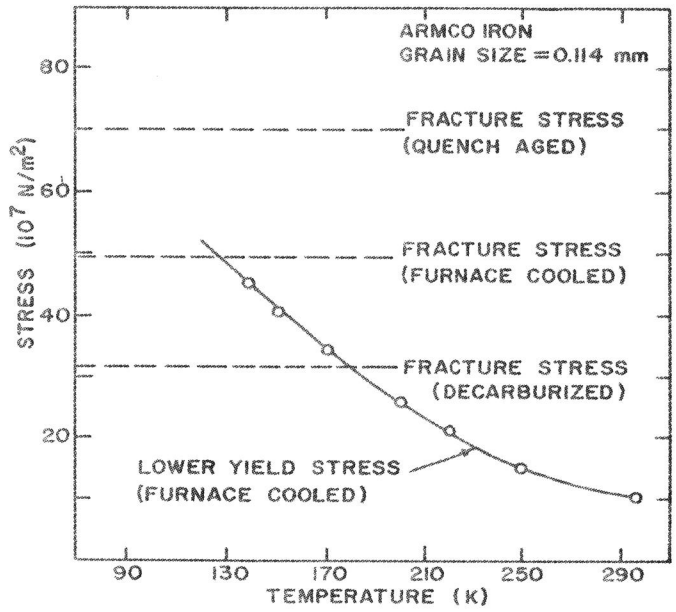

Figure 13 Diagram illustrating the relationship between the fracture stress and the microstructure in Iron.

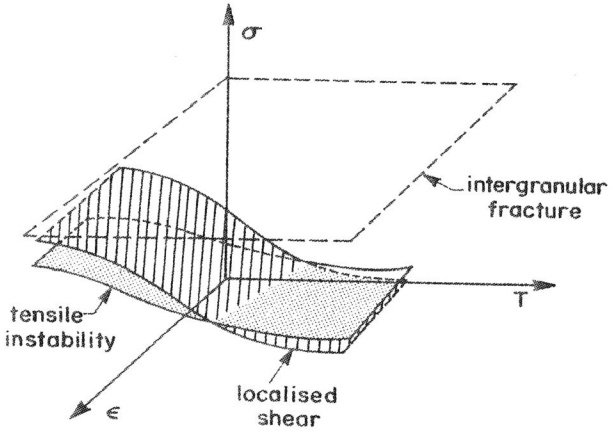

Figure 14 Schematic diagram illustrating the fracture resistance of aluminum alloys. The three common modes of failure are represented as failure surfaces in the 3 dimensional σ - ε - T space. Reference [9].

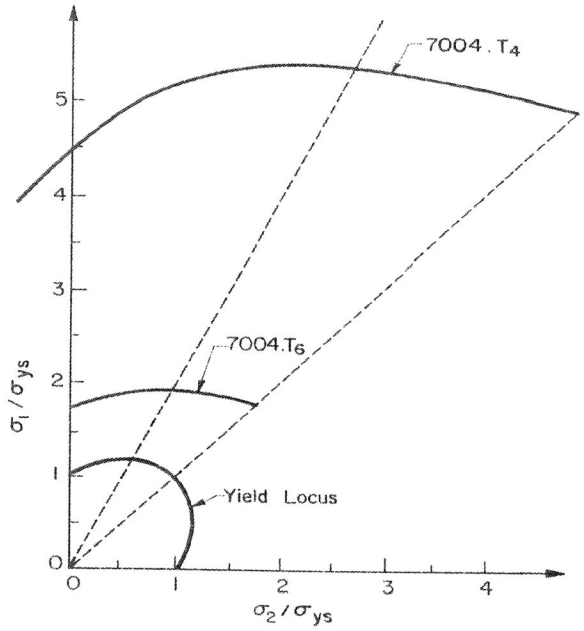

Figure 15 Fracture maps obtained in the case of an Aluminum alloy 7004 for two different heat treatments.

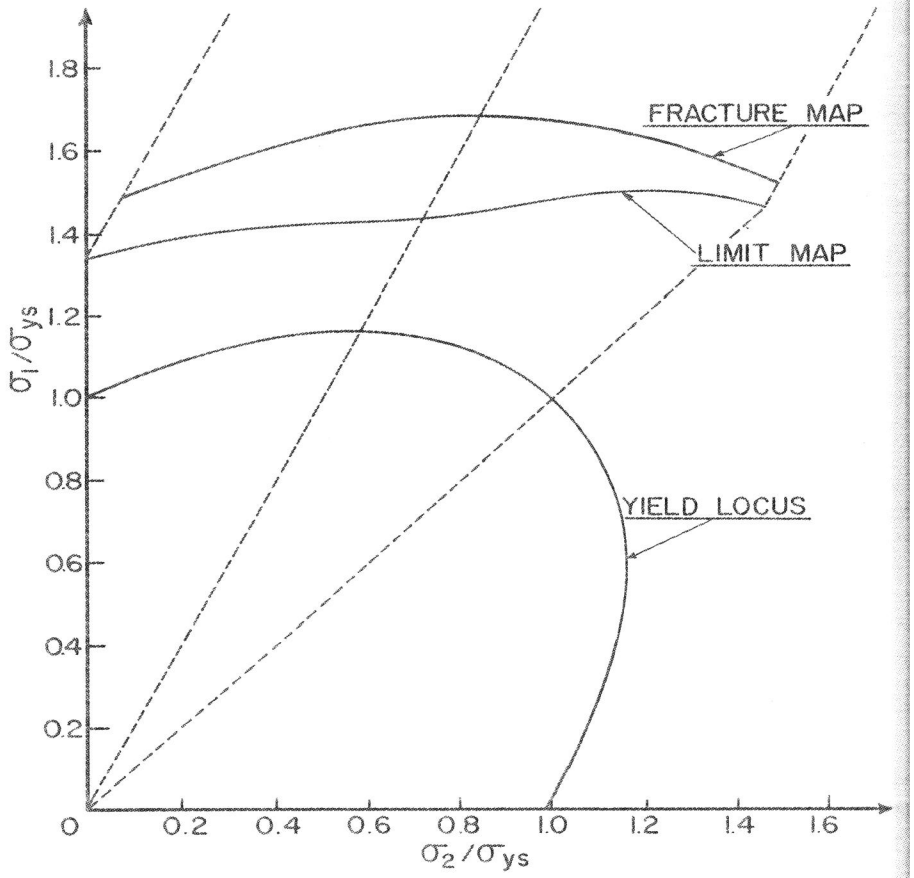

Figure 16 Fracture map obtained in the case of an ultra fine grained aluminum alloy.